energies

MDPI

Article

Application-Oriented Optimal Shift Schedule Extraction for a Dual-Motor Electric Bus with Automated Manual Transmission

Mingjie Zhao [1], Junhui Shi [2], Cheng Lin [1,*] and Junzhi Zhang [2]

1 National Engineering Laboratory for Electric Vehicles, School of Mechanical Engineering, Beijing Institute of Technology, Beijing 100081, China; bitzmj@163.com

2 State Key Laboratory of Automotive Safety and Energy, Tsinghua University, Beijing 100084, China; shijunhui@huachuangev.com (J.S.); jzhzhang@mail.tsinghua.edu.cn (J.Z.)

* Correspondence: lincheng@bit.edu.cn; Tel.: +86-10-6891-3992

Received: 26 December 2017; Accepted: 29 January 2018; Published: 2 February 2018

Abstract: The conventional battery electric buses (BEBs) have limited potential to optimize the energy consumption and reach a better dynamic performance. A practical dual-motor equipped with 4-speed Automated Manual Transmission (AMT) propulsion system is proposed, which can eliminate the traction interruption in conventional AMT. A discrete model of the dual-motor-AMT electric bus (DMAEB) is built and used to optimize the gear shift schedule. Dynamic programming (DP) algorithm is applied to find the optimal results where the efficiency and shift time of each gear are considered to handle the application problem of global optimization. A rational penalty factor and a proper shift time delay based on bench test results are set to reduce the shift frequency by 82.5% in Chinese-World Transient Vehicle Cycle (C-WTVC). Two perspectives of applicable shift rule extraction methods, i.e., the classification method based on optimal operating points and clustering method based on optimal shifting points, are explored and compared. Eventually, the hardware-in-the-loop (HIL) simulation results demonstrate that the proposed structure and extracted shift schedule can realize a significant improvement in reducing energy loss by 20.13% compared to traditional empirical strategies.

Keywords: dual-motor-AMT electric bus (DMAEB); energy management strategy; dynamic programming (DP); shift schedule extraction method; hardware-in-the-loop (HIL)

1. Introduction

To tackle the increasingly serious environmental pollution and energy shortage, the development of electric vehicles (EVs) is recognized as one of the most promising solutions. With the rapid progress of power battery technology [1,2], battery electric vehicles (BEVs) show great advantages in public transportation owing to their zero emissions and fossil fuel consumption [3,4]. Although BEVs can be driven directly by a single motor with the single-stage reducer, the disadvantages of this simple configuration are obvious, such as the steep demand of the high performance motor and the low ability of adapting to various road conditions. To meet the high torque requirement at continuous uphill terrains and high-speed range [5], the BEVs equipped with automated mechanical transmission (AMT) play an important role in satisfying such objectives [6]. However, the conventional AMT propulsion system integrated with single motor has considerable traction interruption resulting in a bad ride comfort and longer acceleration time [7].

Besides a proper configuration for specific EVs, the energy management strategies, especially the gear shift schedule, strongly influence the energy consumption economy and the comprehensive property. These strategies can be generally classified into rule-based control strategy and optimization-based control strategy [8,9]. The former can be easily developed through practical engineering experience and can be executed rapidly in real-time [10]. However, rule-based strategies require to be established in advance merely based on some empirical knowledge, which demands amount of experiment results [11,12]. Thus, research on global optimal energy management algorithm has aroused great interest recently, such as genetic algorithm (GA) [13], particle swarm optimization (PSO) [14] and dynamic programming (DP) [5,8,10,15]. The methods above can lead to the optimization results theoretically, but can neither be implemented in practical directly nor reach an efficient energy cost result virtually.

According to the analysis of practical application in vehicle road test scenario and theoretical simulation results in latest literature research [16–18], three critical factors can be determined, which will influence the effect of actual implementation. First, the transmission efficiency of AMT system is usually ignored or set to an experiential constant in advance. This will result in inherent errors in such systematic optimization problems. In addition, the real efficiency characteristics of different gears is prominent in EVs propulsion system since the motor efficiency is always higher than 90% [19]. Second, the shift process of AMT is ignored, which means the gears can be switched to each other in a single simulation step without any reasonable delay [6]. To neglect the details in shift process is a necessary simplification to focus on the energy problem [20], but such consequence will mislead the real gear shift control sequence in practice. Third, the results of global optimization algorithm are only the optimal working points under certain drive conditions, but in actual the specific gear shift schedule should be extracted so that can be employed in real-time. However, a general precise optimal rule-based strategy extraction method is hard to explore, since the optimal working points is scattered and irregular [21]. Some related studies have been conducted on the rule extraction issue: Shen, W. et al. [15] eliminate irregular points directly and draw various gear shift boundaries based on intuition from DP results. However, this solution will reduce the effect of global optimization and also need much subjective experience to calibration. Peng, J. et al. [22] point out that it is very hard to get the ideal distribution line and definite an optimized working area according to DP results as the improved strategy. The performance seems significant but still leaves much room to improve. An online intelligent energy controller for power split is built, which mainly consists of two neural network (NN) modules trained by DP results [23]. Though the numerical simulation results show a significant energy-saving effect, the response speed and performance in practical application is not validated, which is normally cumbersome.

To deal with the aforementioned problems, a novel dual-motor coupled with 4-speed AMT propulsion system is proposed for electric bus in this paper, which can eliminate the down-to-zero traction interruption of traditional AMT [24]. Basic configuration and working principle of the dual-motor-AMT electric bus (DMAEB) are introduced and DP algorithm is applied to find the optimized gear shift strategy. Additionally, the related shift process characteristics are studied based on bench test to improve the practicability of the optimization, i.e., different gear efficiency maps are considered and the accurate shift time between adjacent gears are determined. The main contribution in this study is to develop and compare proper methods to extract the optimal gear shift schedule from the DP results, which are based on non-linear support vector machine (SVM) classifier and hierarchical clustering (HC) algorithm. Hardware-in-the-loop (HIL) tests are employed furtherly to verify the energy-saving performance of the extracted shift rules.

The remainder of this study is arranged as follows: In Section 2, the novel configuration of DMAEB is presented and the detailed longitudinal dynamic model of the powertrain based on bench test data is built. State formulas, cost function and necessary constrains are discussed in detail and DP algorithm for DMAEB energy optimization is implemented in Section 3. Section 4 introduces two novel extraction methods, which are used to establish an optimal shift schedule according to the DP results. In Section 5, HIL test is employed to validate the real-time energy-saving effect of the extracted gear shift schedule and the results of energy consumption are compared. The last Section gives a brief conclusion of this study.

2. Configuration and Modelling of the DMAEB Powertrain

Figure 1 shows the powertrain structure of the DMAEB studied in this paper. The main power supplier of DMAEB is a single-shaft propulsion system consisting of two motor/generators (MG1 and MG2) and a 4-speed AMT gearbox. The MG2 is connected directly to the drive axle and the MG1 is joint to the AMT. To achieve better dynamic coupling, the output shaft of AMT is arranged to the rotator of MG2 coaxially. Thus, when MG1 unloads torque and starts to regulate speed in shift process [25], MG2 can still output appropriate torque to inhibit the shift impact and avoid the down-to-zero traction interruption. The powertrain will be implemented on a 12-m bus and the main parameters based on coasting test can be seen in Table 1. As this work is focused on the energy economy problem, the model of the powertrain including the two MGs, AMT, battery and vehicle longitudinal dynamics will be rationally simplified and can be described as follows.

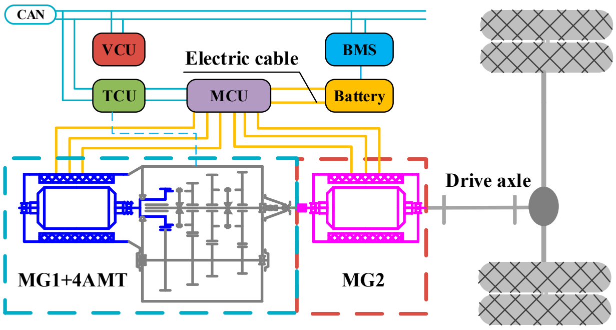

Figure 1. The powertrain configuration of the dual-motor-AMT electric bus (DMAEB) including controller area network (CAN), vehicle control unit (VCU), traction control unit (TCU), motor control unit (MCU), and battery management system (BMS).

Table 1. Main parameters of the dual-motor-AMT electric bus (DMAEB).

Symbol	Parameters	Values
M	Gross weight	18,000 kg
m	Curb weight	12,500 kg
r	Tire rolling radius	0.465 m
a	Constant term of driving resistance	814.2 N
b	Linear term of driving resistance	7.244 N/(km/h)
c	Quadratic term of driving resistance	0.261 N/(km/h)^2
i_0	Main reducer ratio	5.24
η_T	Overall powertrain efficiency	0.95
δ	Rotating mass coefficient	1.02

2.1. Motor/Generator Model

The two MGs are both permanent magnet synchronous motor (PMSM) and can work in energy recovery mode. The peak power (peak torque) of MG1 and MG2 are, respectively, 140 kW (900 Nm) and 90 kW (860 Nm) and the maximum speed of these two motors are both 3000 rpm. The motor efficiency can be modeled through preset maps related to the MGs output rotation speed and torque as shown in Figure 2a,b, which are obtained by bench test in advance. Thus, the output power can be described as follows:

$$P_{MG} = T_{MG} \cdot \omega_{MG} \cdot \eta_{MG}^{-sgn(T_{MG})} / 9549 \tag{1}$$

where P_{MG} presents the power of the MGs, T_{MG} and ω_{MG} are the torque and rotation speed of the motors; the motor efficiency η_{MG} can be found by a 2-D lookup table related to the rotation speed ω_{MG} and the torque T_{MG}; the number 9549 is a unit conversion factor which can transform the popular units to international units.

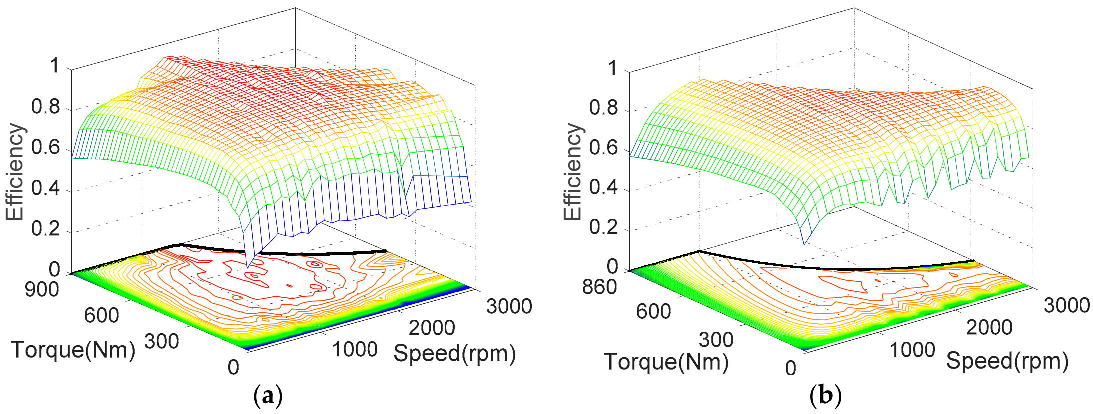

Figure 2. Motor efficiency map based on bench test. (**a**) Efficiency map of Motor/Generator 1; (**b**) Efficiency map of Motor/Generator 2.

2.2. Automated Mechanical Transmission Bench Test and Model

The automated mechanical transmission (AMT) is very important in the powertrain and can directly influence the output characteristic of MG1. According to the requirement of typical bus drive cycle, the 4-speed gear ratio can be set as $i_g = \{3.896, 2.427, 1.483, 1\}$. Then the MG1 equipped with AMT system can be shown as follows:

$$\begin{cases} T_{AMT} = T_{MG1} \cdot i_g \\ \omega_{AMT} = \omega_{MG1} / i_g \end{cases} \tag{2}$$

To ensure the actual implementation effect, bench test of MG1–AMT assembly system as shown in Figure 3 is conducted to find out the efficiency characteristics of different gears and the impact of real shift process. Here the gear switching actuator is much more powerful than the gear engaged friction proportional to the load, which means the real vehicle load and the gear release time in shifting process can be ignored. Considering the real velocity will not change suddenly, a smaller flywheel with 70 kg·m^2 rotation inertia is arranged to simulate the approximate constant output speed in gear shifting process.

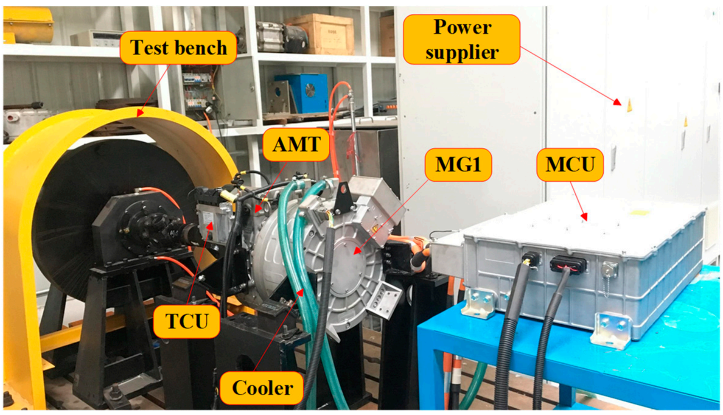

Figure 3. Test bench of MG1–Automated Manual Transmission (MG1–AMT) assembly system.

The gear shift time is an aggregative indicator to show the influence of the shift process in energy management programming. To avoid systematic errors, millions of times of dynamic shift tests have been done and the typical results are shown in Figure 4. From which we can see that the longest shift time cost occurs in the switching between gear 2 and gear 3 and the maximum shift time is about

1.4 s. Besides, the average and minimum shift time of different gears are quite similar, which are about 0.8 s and 0.6 s, respectively. Though shift failure and remedy scenario can result in a long shift time, the frequency is so low that it can be ignored in common control strategy. Therefore, the shift time delay should be set to 3 s to guarantee the gear shift in optimization is applicable. Considering the braking time of bus from 80 km/h to stop is less than 5 s [26], the gear shift in braking process is valueless and even loss more regenerated energy due to power interruption of MG1.

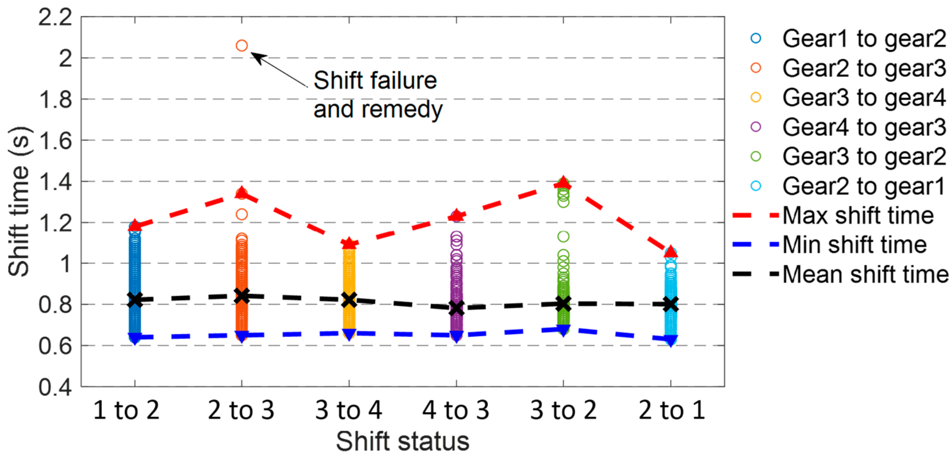

Figure 4. Shift time between different gears.

To describe the shifting process of AMT considering the limits above, a discrete-time dynamic system is modeled as Equations (3)–(5).

$$i_{g,k} = \begin{cases} 3.896 & gear_k = 1 \\ 2.427 & gear_k = 2 \\ 1.483 & gear_k = 3 \\ 1 & gear_k = 4 \\ 0 & gear_k = 0 \end{cases} \tag{3}$$

$$gear_{k+1} = \begin{cases} 4 & gear_k + shift_k > 4 \\ 0 & gear_k + shift_k < 0 \\ gear_k + shift_k & others \end{cases} \tag{4}$$

$$shift_k = \begin{cases} f(\alpha_{acc}, v) = \{-1, 0, 1\} & T_d \geq 3, T_{req} \geq 0 \\ 0 & T_d < 3, T_{req} < 0 \end{cases} \tag{5}$$

where $gear_k$ is AMT current operating gear status and $shift_k$ is AMT shift commands which is constrained to be selected from the values of $\{-1, 0, 1\}$ denoting downshift command, sustain command and upshift command according to accelerating position α_{acc} and velocity v. T_d is the shift time counter whose threshold is 3 s. T_{req} is the required torque, which can be positive or negative values according to drive conditions.

The output and efficiency characteristics can be seen in Figure 5. Here, we can find that the different gears will influence the value of efficiency a little but will change the distribution observably. The transmission efficiency from gear 1 to gear 4 increases moderately. The location and proportion of high efficiency area are different from each other, where gear 1 and gear 3 reach a smaller high efficiency area than gear 2 and gear 4. To promote the accuracy as possible, four 2-D lookup tables should be built and applied to describe the real performance of MG1–AMT assembly system.

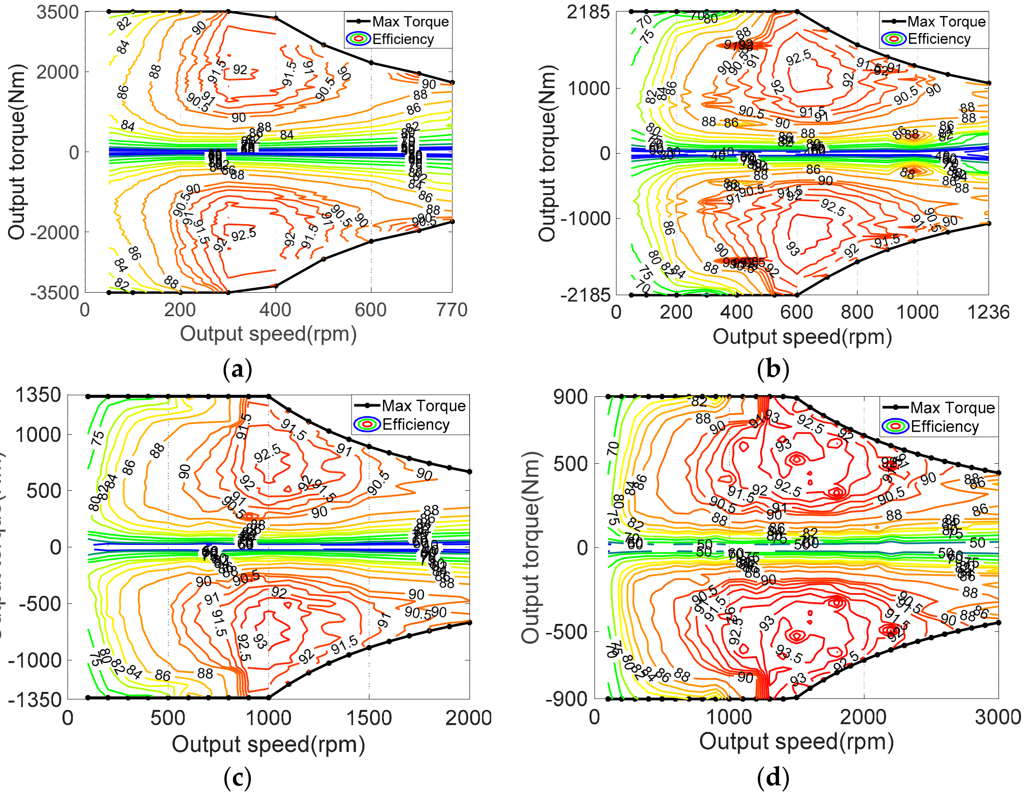

Figure 5. Efficiency map of MG1–AMT assembly system. (**a**) Efficiency map of gear 1; (**b**) Efficiency map of gear 2; (**c**) Efficiency map of gear 3; and (**d**) Efficiency map of gear 4.

2.3. Battery Model

To simplify the optimization problem, the impact of temperature and the internal reaction of the battery are ignored. An effective static equivalent circuit battery model is used [27,28] and transformed to a discrete-time state of charge (*SOC*) model that can be described as:

$$SOC_{k+1} = SOC_k - \frac{V_{oc,k} - \sqrt{V_{oc,k}^2 - 4(R_{\text{int},k} + R_t) \cdot P_{bat,k}}}{2(R_{\text{int},k} + R_t) \cdot C} \quad (6)$$

$$P_{bat,k} = (P_{AMT,k} + P_{MG2,k})\eta_{bat,k}^{-sgn(P_{AMT,k}+P_{MG2,k})} \quad (7)$$

where $V_{oc,k}$ is the open-circuit voltage, $R_{int,k}$ is the internal resistance of the battery, and these parameters are related to *SOC* and can be determined by a lookup table; $R_{t,k}$ is the terminal resistance which can be defined as a constant, C is the maximum battery capacity; $P_{bat,k}$ is the power of battery which can be calculated by $P_{AMT,k}$, $P_{MG2,k}$ and the efficiency $\eta_{bat,k}$.

2.4. Vehicle Longitudinal Dynamic Model

According to analysis of the vehicle longitudinal dynamics shown in Figure 6, the drive force provided by the coupling propulsion system should balance the resistance force as shown in Equation (8). Thus the basic discrete-time velocity variation can be determined as Equation (9).

$$\begin{cases} T_{req}/r = F_a + F_f + F_w + F_i \\ T_{req} = (T_{MG2} + T_{MG1} \cdot i_g) \cdot i_0 \cdot \eta_T + T_{brk} \end{cases} \quad (8)$$

$$v_{k+1} - v_k = [(T_{MG2,k} + T_{MG1,k} \cdot i_{g,k}) \cdot i_0 \cdot \eta_T + T_{brk} - (F_{a,k} + F_{f,k} + F_{w,k} + F_{i,k})r]/\delta mr \quad (9)$$

where T_{req} is the required torque; T_{brk} is the total mechanical braking torque on the wheels; F_a is the acceleration resistance, F_i is the gradient resistance, and F_f and F_w are the rolling resistance and the aerodynamic drag resistance, which can be calculated by the driving resistance fitting function.

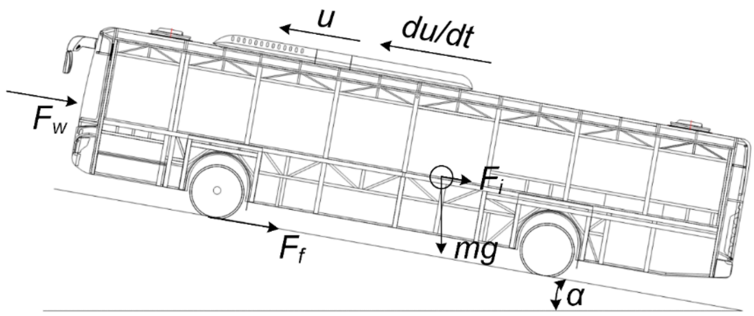

Figure 6. The analysis of vehicle longitudinal dynamics.

3. Optimal Energy Management Based on Dynamic Programming

Dynamic programming (DP) algorithm is based on Bellman principle of optimality [12]. Thus, it can always find the optimal energy consumption results effectively and consider the essential constraints when handling the DMAEB energy management. Herein, a numerical-based DP method is employed to solve the energy-saving optimization and find the optimal gear shift schedule over a definite driving cycle.

3.1. Problem Formulation of the DMAEB Gear Shift Schedule

For DMAEB gear shift schedule optimization, DP aims to arrange the certain gear status in each stage to minimize the total cost over the whole driving cycles. Therefore, the state variables and control variables should be determined to formulate the DP problem. The state variables and control variables should be as few as possible to reduce the computation burden, which means only the independent and uncertain variables should be taken into consideration. So only the SOC and gear status $gear_k$ are selected as the state variables, and the torque of MG2 $T_{MG2,k}$ and AMT shift command $shift_k$ are chosen as the control variables. Hence, the state equation of DMAEB can be determined in a discrete-time format as:

$$\begin{cases} X_{k+1} = f(X_k, U_k) \\ X_k = [SOC_k \quad gear_k] \\ U_k = [T_{MG2,k} \quad shift_k] \end{cases} \tag{10}$$

where X_k is state variable vector of the powertrain and U_k is the control variable vector, the simulation step here is set as 1 s.

As all the variables above have certain limits so that the constraints in Equation (11) are necessary to ensure a smooth and rational operating of the powertrain [29]. Here the rotation speed of motors $\omega_{MG*,k}$ should be limited and proportional to vehicle speed; the output torque $T_{MG*,k}$ should be restricted according to power limits and meet the demand of driving; SOC_k should be constrained to protect the battery.

$$\begin{cases} \omega_{MG*,\min} \le \omega_{MG*,k} \le \omega_{MG*,\max} \\ T_{MG*,\min}(\omega_{MG*,k}, SOC_k) \le T_{MG*} \le T_{MG*,\max}(\omega_{MG*,k}, SOC_k) \\ \begin{cases} (T_{MG2,k} + T_{MG1,k} \cdot i_{g,k}) \cdot i_0 \cdot \eta_T + T_{brk,k} = T_{req,k} & gear_k \neq 0 \\ T_{MG2,k} \cdot i_0 \cdot \eta_T + T_{brk,k} = T_{req,k} & gear_k = 0 \end{cases} \\ \begin{cases} \omega_{MG2,k} = \omega_{MG2,k}/i_{g,k} = u_k/3.6/r/i_0 & gear_k \neq 0 \\ \omega_{MG2,k} = u_k/3.6/r/i_0 & gear_k = 0 \end{cases} \\ SOC_{\min} \le SOC_k \le SOC_{\max} \end{cases} \tag{11}$$

In order to match the actual situation, a penalty factor is added to avoid the frequent gear shift phenomenon. Therefore, the optimization goal is to find a certain control sequence to minimize the battery energy cost considering the frequency of shift and the constraints as:

$$J = \sum_{k=0}^{N-1} L(X_k, U_k) = \sum_{k=0}^{N-1} (EC_k + \beta \times |shift_k|) \tag{12}$$

where N is the total duration of driving cycle; L is the instantaneous cost; EC_k denotes the battery energy cost at each stage; β is set as a penalty factor to reduce shift frequency.

3.2. Implementation of DP Method Solving the Optimization Problem

The global optimization problem can be divided into a sequence of sub-problems backward from the terminal stage [8]. As the DMAEB propulsion system is a continuous nonlinear model, the state space should be transformed to discrete numerical form totally. Then, DP problem can be described by the recursive equations. For step $(N-1)$ the equation is:

$$J^*_{N-1}(X_{N-1}) = \min_{U_{N-1}} [L(X_{N-1}, U_{N-1})] \tag{13}$$

And for step k $(0 \leq k < -1)$, the equation is:

$$J^*_k(X_k) = \min_{U_k} [L(X_k, U_k) + J^*_{k+1}(X_{k+1})] \tag{14}$$

where $J^*_k(X_k)$ is the optimal cost function at stage X_k from step k to the terminal of the driving cycle and X_{k+1} is the $(k+1)$ state after the control variable at former stage is propelled to state X_k according to Equation (10).

To solve the above recursive backward rapidly and accurately, the state X_k and control variables U_k should be discretized into finite enough grids and interpolation method is used to evaluate the values aside the grids. The resolution of state and control variables influences the accuracy of the optimization and the computational cost significantly. As the solution is obtained mostly offline, minute grids can be implemented to solve the DP problem backward in order to guarantee the control performance. To accelerate the computing process, the longitudinal dynamic function-solving problem can be replaced by discrete wheel-side required torque sequence $T_{req,k}$ and axle speed sequence $\omega_{req,k}$ by calculating the required power and torque of DMAEB in a certain driving cycle in advance. Afterwards the optimal control law will be determined forward.

4. Extraction Methods of Implementable Gear Shift Schedule

4.1. Discussion on Gear Shift Frequency and Energy Loss

To explore the comprehensive potential of DMAEB and find a general optimal shift schedule, the Chinese-World Transient Vehicle Cycle (C-WTVC) as shown in Figure 7 is employed in the DP procedure mentioned above. The C-WTVC is a typical driving cycle designed for heavy-duty commercial vehicle, which consists of urban and highway driving conditions in rational proportion. The total driving distance is 20.51 km and the driving time is 1800 s. Since the routine of city bus is always determined in advance and similar to the typical cycles, so it is suitable to adopt C-WTVC to extract the optimal gear shift schedule. Further, a certain city routine can be surveyed and implemented to design the specific shift maps in practical real vehicle application.

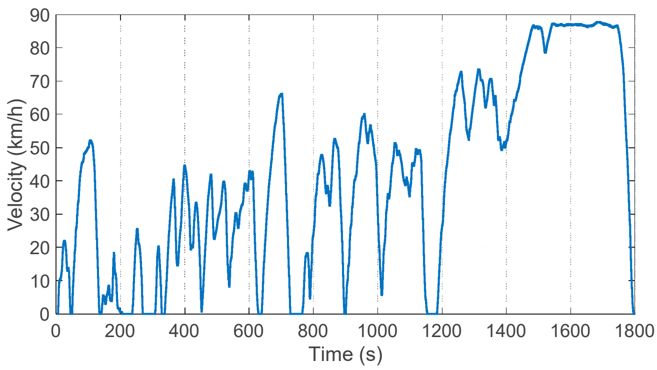

Figure 7. The profile of Chinese-World Transient Vehicle Cycle (C-WTVC).

As presented in Figure 8, if the shift time delay is neglected, DP will try to find the abstractly optimal results by switching the gears in each stage, but such high shift frequency is useless in real application. To avoid this phenomenon, the aforementioned shift time delay is integrant. Besides, a proper shift frequency penalty factor will make a trade-off between the energy loss and the number of shifts. The penalty factor is varied by degrees as $\beta = \{0, 1, 5, 10, 20, 50, 100, 200\}$ and its influence on energy loss and number of shifts in accelerating process are presented in Figure 9. Here we can see that with the increase of β the number of shifts is declining and the energy loss is rising. However, when $\beta > 20$ the trend will come to a standstill gently. So the proper value should be $\beta = 20$ with only 21 times gear shift as shown in Figure 10 and the minimum gear shift interval is 10 s, which is applicable in real shift process. The *SOC* variation is illustrated in Figure 11, where the initial *SOC* is set to 90.0% and in the end of the 20.51 km driving cycle it only reduces to 81.31%.

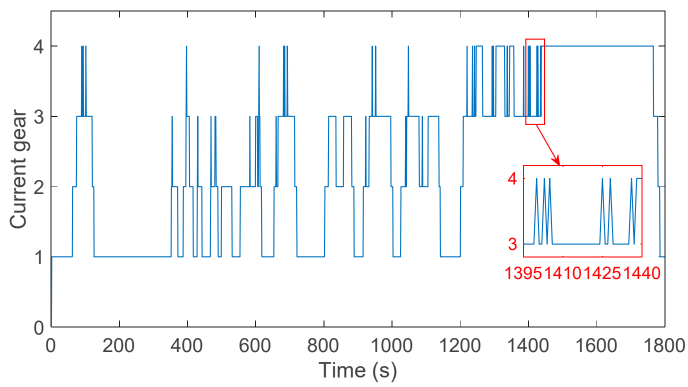

Figure 8. Gear shift status under dynamic programming (DP) method without shift time delay.

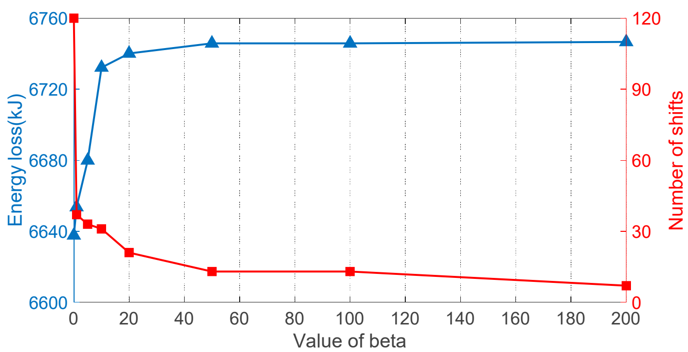

Figure 9. The influence of different β on the energy loss and number of shifts.

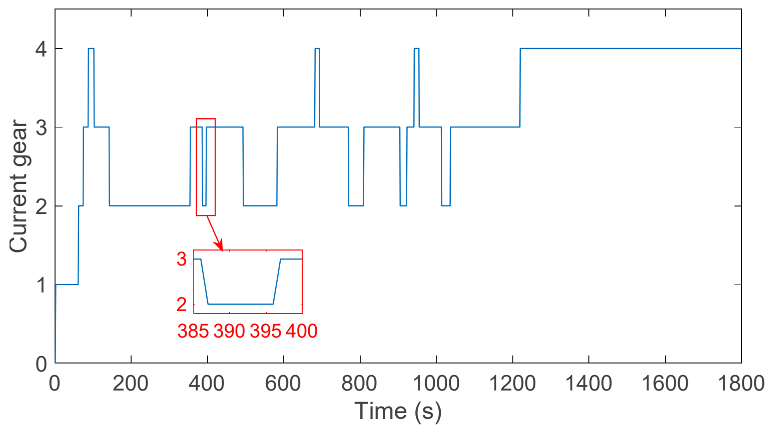

Figure 10. Gear shift status under DP method with 3 s shift time delay and $\beta = 20$.

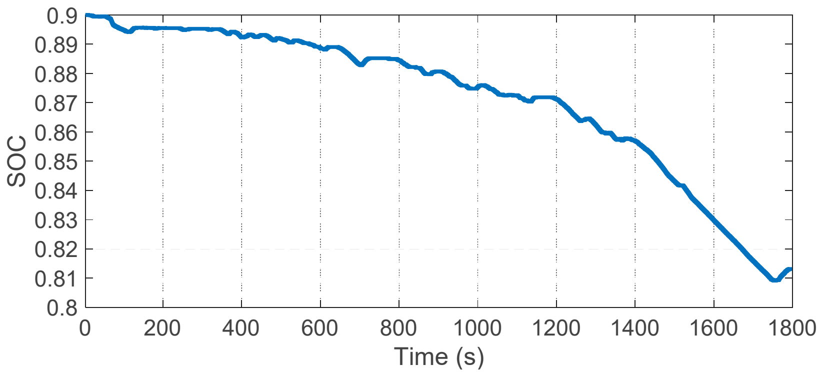

Figure 11. State of Charge (SOC) variation trend of C-WTVC under DP method with $\beta = 20$.

4.2. Development of Optimal Gear Shift Schedule Extraction Methods

It is obvious that DP method cannot be utilized to handle global optimization problem online due to its computational burden and demand of prescient routine. However, the results of DP provide with lots of valuable features, which can guide the optimal rule extraction. There are two aspects of features, which are related to the gear shift problem, i.e., the optimal gear operating points and the optimal gear shifting points. In addition, these optimal points afford two distinct perspectives of shift schedule extraction, which are the classification method and the clustering method.

Intuitively, the boundaries of optimal operating points are the desired shift schedule. However, it is impossible to find such boundaries reasonably without any empirical pretreatments, since the optimal operating points are strongly irregular and intersecting as shown in Figure 12a. To some extent, the shift schedule extraction can be equivalent to a classification problem. After separating the points in adjacent gears form, the schedule problem can be converted to a linear inseparable binary classification problem. Many tools have been developed to solve the classification problem, and among them the support vector machine (SVM) is a useful kernel-based method for binary classification [30]. The basic principle of SVM is to convert linear inseparable input space to a high dimensional feature space utilizing Kernel Functions (KFs), which meet the Mercer's condition [31]. The input dataset should be given as:

$$\left\{\left(\vec{x}_1, y_1\right), \left(\vec{x}_2, y_2\right), \ldots, \left(\vec{x}_k, y_k\right), \ldots, \left(\vec{x}_n, y_n\right)\right\} \tag{15}$$

where $\vec{x}_k$ is the input vector, i.e., the optimal gear operating points, y_k is the gear status to be classified and n is the total number of the samples.

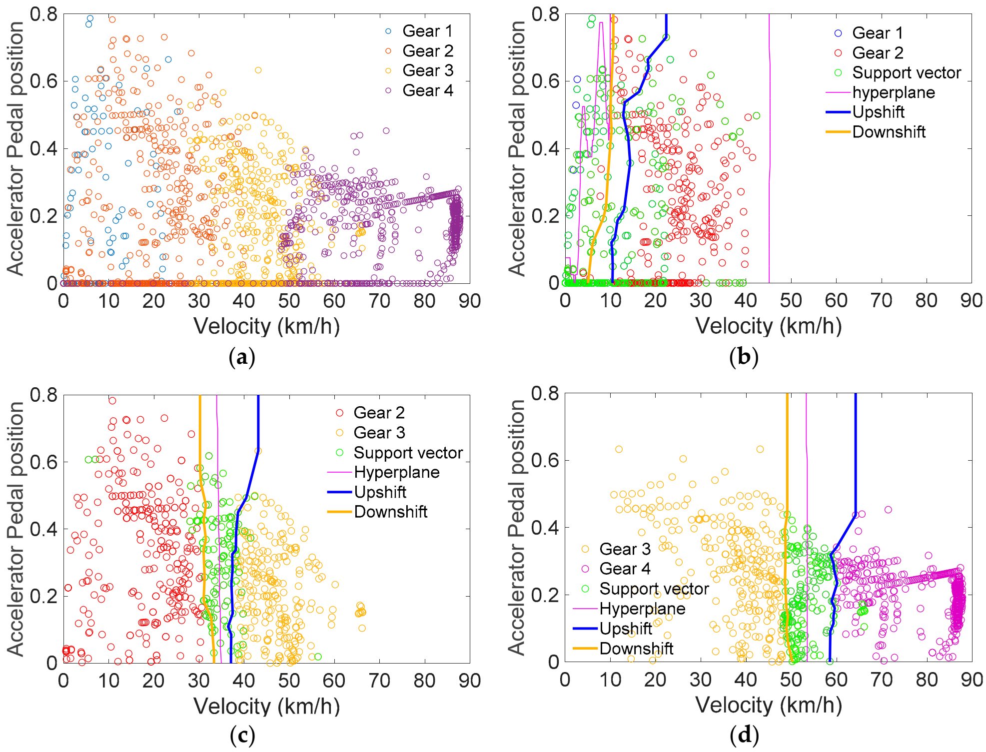

Figure 12. The process of optimal shift schedule extraction by SVM. (**a**) Gear operating points allocation in accelerating process; (**b**) Gear 1 to gear 2 extraction based on γ = 1.8, C = 120 Radial Basis Function (RBF) kernel classification; (**c**) Gear 2 to gear 3 extraction based on γ = 15, C = 50 RBF kernel classification; and (**d**) Gear 3 to gear 4 extraction based on γ = 10, C = 50 RBF kernel classification.

The target of SVM method is to obtain an optimal hyperplane that can minimize the upper bound of generalization error as shown in Equation (16).

$$g\left(\vec{x}\right) = w^T\vec{x} + b = 0 \tag{16}$$

where ω and b are the normal vectors of the hyperplane, which can be calculated by maximizing the margin between the separating hyperplane and the input data.

Considering the ambiguous boundary of the points, a relaxation factor can be adopted to relax the constraints and the maximum problem can be described as:

$$\begin{cases} \underset{\alpha}{\text{argmax}} Q(\alpha) = \underset{\alpha}{\text{argmax}} \sum\limits_{i=1}^{n} \alpha_i - \dfrac{1}{2} \sum\limits_{i=1}^{n} \sum\limits_{j=1}^{n} \alpha_i \alpha_j y_i y_j K(X_i, X_j) \\ s.t. \quad 0 \le \alpha_i \le C, i = 1, \cdots, n \\ \qquad \sum\limits_{i=1}^{n} \alpha_i y_i = 0 \end{cases} \tag{17}$$

where α_i is the Lagrange coefficient, C is a penal factor to reduce the impact of relaxation, $K(X_i, X_j)$ is the Kernel function. Here, the most effective KF is the Radial Basis Function (RBF) as:

$$K(x, y) = e^{-\gamma \|x-y\|2} \tag{18}$$

The result of SVM classification can be seen in Figure 12b–d, where the hyperplane can indicate the trend of the boundaries and the support vectors can determine the optimal separations of the points. According to real engineering application, the practical downshift and upshift schedules in accelerating process can be determined by fitting the proper support vectors.

Another extraction method is to cluster the optimal shifting points, as shown in Figure 13a. As the applicable shift schedule are single switching lines, the centralized line of these optimal shifting points will lead to the desired shift rules.

Hierarchical clustering (HC) is an adaptive method to cluster these points layer by layer and finally can single out the points to fit the optimal shift lines. The details of HC method can be seen in Ref. [32]. However, in this study the optimal shifting points are rare and distinct since the gear shift frequency is limited. Hence the upshift schedule can be extracted directly by fitting the shifting points between different gears as shown in Figure 13b.

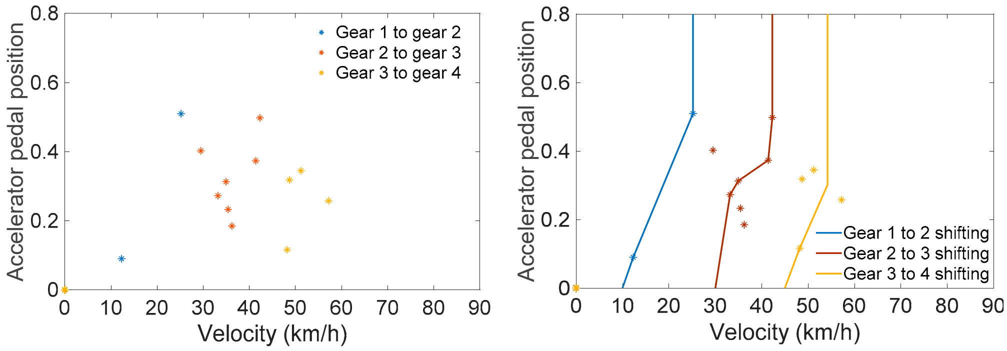

Figure 13. The process of optimal shift schedule extraction by clustering. (**a**) Gear shifting points allocation in accelerating process; (**b**) Upshift schedule based on clustering.

4.3. Compare of the Classification and Clustering Extraction Methods

Considering the power performance in high accelerator pedal position, the final optimal gear shift schedules extracted by the methods above are shown in Figure 14. Here we can see that the classification results are more detailed and the clustering results are cursory whose downshift schedule have to be drawn according to experience. Though the effect of extraction will mainly depend on the number of optimal data, the intricate points will increase the difficulty of extraction.

Additionally, the inherent features of these two methods are distinct. The classification will always handle much data and is good at clarifying the detail trend of the boundaries. However, the clustering method will focus on the important shifting points, which can find the basic boundaries efficiently and easily. We can extract the shift schedule by two methods and choose the better one leading to a low energy consumption. Also, the two results can be considered together as a reference to guide the calibration of real vehicle control online.

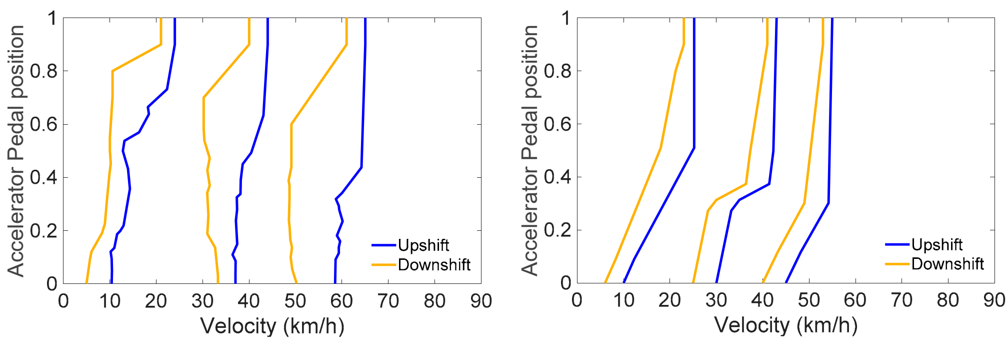

Figure 14. Optimal gear shift schedule extraction results. (**a**) Optimal schedule based on classification; (**b**) Optimal schedule based on clustering.

5. Analysis of Results Based on Hardware-in-the-Loop Tests

5.1. Hardware-in-the-Loop Test Bench

Hardware-in-the-loop (HIL) test is an efficient technology in the process of modern automotive development. Admittedly, dSPACE is the leading producer of engineering tools for HIL test especially in automotive industry. It can not only provide a powerful hardware which can calculate and simulate the vehicle status very well but also make it convenient to realize strategies through its software embedded in the MATLAB/Simulink environment. In this study, the test is mainly based on the dSPACE (Digital signal processing and control engineering GmbH, Paderborn, Germany) simulator and its toolchains.

The extracted shift schedule of DMAEB is easy to be established in Simulink environment and then Embedded Coder tools are employed to convert the strategy in C language. After that, the model-in-the-loop (MIL) and software-in-the-loop (SIL) tests are conducted at first to prepare for the HIL test. As the infrastructure development and application programming interface (API) have been designed already, the strategy in C language can be downloaded to a beforehand vehicle control unit (VCU). The vehicle model is built in MATLAB/Simulink software (The MathWorks, Inc., Natick, MA, USA), the interfaces and CAN bus communication protocol of HIL is defined by CAN blockset in real-time interface (RTI) tool of dSPACE. The model can be complied and downloaded into Autobox simulator platform by ControlDesk software of dSPACE.

The VCU and Autobox simulator can communicate with each other through the CAN network, where the basic control signals can exchange. The ControlDesk can simulate the driving behavior according to the given driving cycle information and send the pedal position signals to the DMAEB model. A Kvaser CAN card and the relevant upper monitor are responsible for recording all the messages. The final configuration of the HIL test bench is shown in Figure 15, the shift schedule will be executed by a regular single microcontroller in the real-time environment over the C-WTVC driving cycle.

5.2. HIL Test Results and Analysis

The conventional empirical shift schedule and the optimal shift schedule based on classification and clustering extraction methods are validated in the HIL test bench. The initial *SOC* is set to 90% and the variation of *SOC* over C-WTVC cycle is illustrated in Figure 16. Although the extracted optimal shift schedules applied in real-time cannot reach the DP-based simulation effect, the energy-saving performance is much better than empirical schedule.

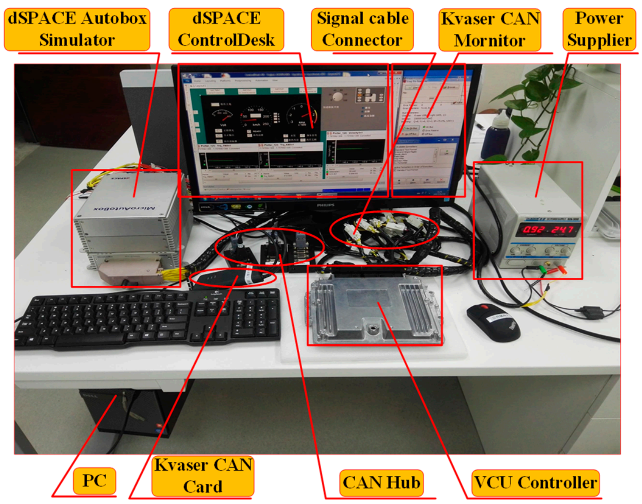

Figure 15. Hardware-in-the-loop (HIL) test bench and related tooltrains.

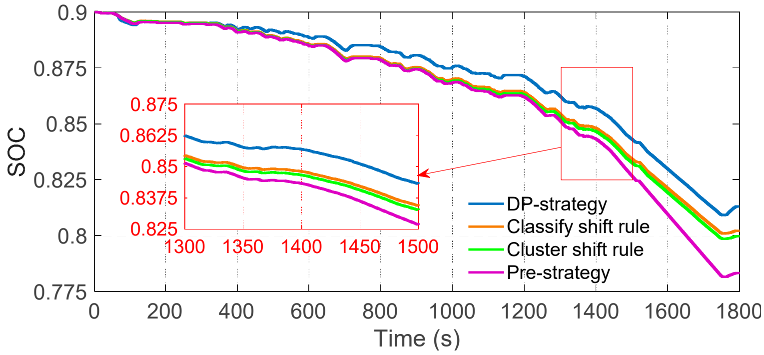

Figure 16. *SOC* variation of different shift schedules over based on HIL tests.

In detail, from start to 1500 s the velocity changes greatly and rapidly, and the optimized shift schedules will lead to a high efficiency gear position, which contributes to the energy-saving performance a lot. From 1500 s to the end the velocity is stabilized but very high, a specific torque distribution of two motors based on DP will result in a high overall efficiency. As the power demand in highway scenario is considerable, the effect of saving energy is obvious. Further, the classification extraction method seems more efficient than the clustering method, since the amount of the sample data made a great contribution. In addition, the extracted rules are executed rapidly by a common VCU in the HIL test, which means they can be applied directly in real vehicles.

The Electricity consumption results over C-WTVC of different shift schedules are shown in Table 2. We can see that the shift schedule based on classification extraction method can result in only about 100 kWh/100 km, which reduces the energy cost by 20.13% compared to that based on the empirical shift schedule.

Table 2. Electricity consumption comparison of different shift schedules.

Control Strategy	Accelerating Consumption kWh/100 km	Braking Consumption kWh/100 km	Total Consumption kWh/100 km
DP method	104.5336	−11.0326	93.5010
Empirical shift rule	136.8763	−10.6701	126.2062
Classify shift rule	111.4997	−10.6963	100.8034
Cluster shift rule	113.3949	−10.0272	103.1877

6. Conclusions

In this paper, a novel dual-motor electric bus with 4-speed AMT configuration is proposed to eliminate the traction interruption in conventional system. The efficiency and shift time of each gear in the MG1–AMT assembly system are considered in detail. The powertrain model of DMAEB is developed and DP algorithm is applied to optimize the gear shift schedule. A reasonable shift time delay based on test results and a penalty factor are set to reduce the shift frequency by 82.5% in C-WTVC driving cycle. Classification and clustering extraction methods are explored and find the implementable optimal shift schedules respectively. The former can clarify the detail trend of the boundaries depends on operating points and the latter can find the basic boundaries efficiently and easily depends on shifting points. HIL tests are conducted and the results demonstrate that the extracted shift schedule can be reliably executed in a common VCU and can improve the energy-saving performance by reducing the electricity consumption by 20.13% compared to the conventional shift schedule. In general, the proposed propulsion system is suitable for transport bus and the two extraction methods can be applied to the design of gear shift schedule in any kinds of vehicles equipped with AMT, which have great potential in practical.

Acknowledgments: This work is supported by the National Key Technology Research and Development Program of China (2017YFB0103801). Any opinions expressed in this paper are solely those of the authors and do not represent those of the sponsors.

Author Contributions: Mingjie Zhao designed the configuration, proposed the algorithms and wrote the paper; Junhui Shi completed the model and simulation; Cheng Lin gave help to the HIL test design and offered financial support; Junzhi Zhang gave many enlightening suggestions about this study.

Conflicts of Interest: The authors declare no conflict of interest.

References

1. Hannan, M.A.; Lipu, M.S.H.; Hussain, A.; Mohamed, A. A review of lithium-ion battery state of charge estimation and management system in electric vehicle applications: Challenges and recommendations. *Renew. Sustain. Energy Rev.* **2017**, *78*, 834–854. [CrossRef]
2. Xiong, R.; Zhang, Y.; He, H.; Zhou, X.; Pecht, M. A double-scale, particle-filtering, energy state prediction algorithm for lithium-ion batteries. *IEEE Trans. Ind. Electron.* **2018**, *65*, 1526–1538. [CrossRef]
3. Mahmoudzadeh Andwari, A.; Pesiridis, A.; Rajoo, S.; Martinez-Botas, R.; Esfahanian, V. A review of Battery Electric Vehicle technology and readiness levels. *Renew. Sustain. Energy Rev.* **2017**, *78*, 414–430. [CrossRef]
4. Xiong, R.; Yu, Q.; Wang, L.; Lin, C. A novel method to obtain the open circuit voltage for the state of charge of lithium ion batteries in electric vehicles by using H infinity filter. *Appl. Energy* **2017**, *207*, 341–348. [CrossRef]
5. Liu, Y.; Li, J.; Ye, M.; Qin, D.; Zhang, Y. Optimal Energy Management Strategy for a Plug-in Hybrid Electric Vehicle Based on Road Grade Information. *Energies* **2017**, *10*, 412. [CrossRef]
6. Liu, T.; Zou, Y.; Liu, D. Energy management for battery electric vehicle with automated mechanical transmission. *Int. J. Veh. Des.* **2016**, *70*, 98–112. [CrossRef]
7. Tseng, C.; Yu, C. Advanced shifting control of synchronizer mechanisms for clutchless automatic manual transmission in an electric vehicle. *Mech. Mach. Theory* **2015**, *84*, 37–56. [CrossRef]
8. He, H.; Tang, H.; Wang, X. Global Optimal Energy Management Strategy Research for a Plug-In Series-Parallel Hybrid Electric Bus by Using Dynamic Programming. *Math. Probl. Eng.* **2013**, *2013*. [CrossRef]
9. Xiong, R.; Cao, J.; Yu, Q. Reinforcement learning-based real-time power management for hybrid energy storage system in the plug-in hybrid electric vehicle. *Appl. Energy* **2018**, *211*, 538–548. [CrossRef]
10. Wirasingha, S.G.; Emadi, A. Classification and Review of Control Strategies for Plug-In Hybrid Electric Vehicles. *IEEE Trans. Veh. Technol.* **2011**, *60*, 111–122. [CrossRef]
11. Torres, J.L.; Gonzalez, R.; Gimenez, A.; Lopez, J. Energy management strategy for plug-in hybrid electric vehicles. A comparative study. *Appl. Energy* **2014**, *113*, 816–824. [CrossRef]
12. He, H.; Xiong, R.; Zhao, K.; Liu, Z. Energy management strategy research on a hybrid power system by hardware-in-loop experiments. *Appl. Energy* **2012**, *112*, 1311–1317. [CrossRef]
13. Arabali, A.; Ghofrani, M.; Etezadi-Amoli, M.; Fadali, M.S.; Baghzouz, Y. Genetic-Algorithm-Based Optimization Approach for Energy Management. *IEEE Trans. Power Deliv.* **2013**, *28*, 162–170. [CrossRef]
14. Chen, S.Y.; Hung, Y.H.; Wu, C.H.; Huang, S.T. Optimal energy management of a hybrid electric powertrain system using improved particle swarm optimization. *Appl. Energy* **2015**, *160*, 132–145. [CrossRef]
15. Shen, W.; Yu, H.; Hu, Y.; Xi, J. Optimization of Shift Schedule for Hybrid Electric Vehicle with Automated Manual Transmission. *Energies* **2016**, *9*, 220. [CrossRef]
16. Gao, B.; Liang, Q.; Xiang, Y.; Guo, L.; Chen, H. Gear ratio optimization and shift control of 2-speed I-AMT in electric vehicle. *Mech. Syst. Signal Process.* **2015**, *50–51*, 615–631. [CrossRef]
17. Ruan, J.; Walker, P.; Zhang, N. A comparative study energy consumption and costs of battery electric vehicle transmissions. *Appl. Energy* **2016**, *165*, 119–134. [CrossRef]
18. Newman, K.; Kargul, J.; Barba, D. Development and Testing of an Automatic Transmission Shift Schedule Algorithm for Vehicle Simulation. *SAE Int. J. Engines* **2015**, *8*, 1417–1427. [CrossRef]
19. Karel, H.; Pavel, D. The validity range of PMSM efficiency map regarding its equivalent circuit parameters. In Proceedings of the 2016 17th International Conference on Mechatronics—Mechatronika (ME), Prague, Czech Republic, 7–9 December 2016; pp. 1–7.
20. Lu, X.; Xu, X.; Liu, Y. Simulation of Gear-shift Algorithm for Automatic Transmission Based on MATLAB. In Proceedings of the 2009 WRI World Congress on Software Engineering, Xiamen, China, 19–21 May 2009; pp. 476–480.

21. Vgo, D.V.; Hofman, T.; Steinbuch, M. Improvement of fuel economy in Power-Shift Automated Manual Transmission through shift strategy optimization—An experimental study. In Proceedings of the 2010 IEEE Vehicle Power and Propulsion Conference, Lille, France, 1–3 September 2010; pp. 1–5.
22. Peng, J.; He, H.; Xiong, R. Rule based energy management strategy for a series–parallel plug-in hybrid electric bus optimized by dynamic programming. *Appl. Energy* **2017**, *185*, 1633–1643. [CrossRef]
23. Chen, Z.; Mi, C.C.; Xu, J.; Gong, X.; You, C. Energy Management for a Power-Split Plug-in Hybrid Electric Vehicle Based on Dynamic Programming and Neural Networks. *IEEE Trans. Veh. Technol.* **2014**, *63*, 1567–1580. [CrossRef]
24. Zhao, M.; Shi, J.; Lin, C. Optimal energy management strategy design based on dynamic programming for a dual-motor-AMT coupling-propulsion electric bus. In Proceedings of the International Symposium on Electric Vehicles, Stockholm, Sweden, 13–14 July 2017.
25. Qin, D.T.; Yao, M.Y.; Chen, S.J.; Lyu, S.K. Shifting process control for two-speed automated mechanical transmission of pure electric vehicles. *Int. J. Precis. Eng. Manuf.* **2016**, *17*, 623–629. [CrossRef]
26. Sangtarash, F.; Esfahanian, V.; Nehzati, H.; Haddadi, S.; Bavanpour, M.A.; Haghpanah, B. Effect of Different Regenerative Braking Strategies on Braking Performance and Fuel Economy in a Hybrid Electric Bus Employing CRUISE Vehicle Simulation. *SAE Int. J. Fuels Lubr.* **2008**, *1*, 828–837. [CrossRef]
27. Yu, Q.; Xiong, R.; Lin, C.; Shen, W.; Deng, J. Lithium-Ion Battery Parameters and State-of-Charge Joint Estimation Based on H-Infinity and Unscented Kalman Filters. *IEEE Trans. Veh. Technol.* **2017**, *66*, 8693–8701. [CrossRef]
28. Chen, C.; Xiong, R.; Shen, W. A lithium-ion battery-in-the-loop approach to test and validate multi-scale dual H infinity filters for state of charge and capacity estimation. *IEEE Trans. Power Electr.* **2018**, *33*, 332–342. [CrossRef]
29. Xiong, R.; Tian, J.; Mu, H.; Wang, C. A systematic model-based degradation behavior recognition and health monitor method of lithium-ion batteries. *Appl. Energy* **2017**, *207*, 367–378. [CrossRef]
30. Shao, Y.H.; Chen, W.J.; Deng, N.Y. Nonparallel hyperplane support vector machine for binary classification problems. *Inf. Sci.* **2014**, *263*, 22–35. [CrossRef]
31. Scholkopf, B.; Sung, K.; Burges, C.J.C.; Girosi, F.; Niyogi, P.; Poggio, T.; Vapnik, V. Comparing support vector machines with Gaussian kernels to radial basis function classifiers. *IEEE Trans. Signal Process.* **1997**, *45*, 2758–2765. [CrossRef]
32. Julio, F.N. A Universal Density Profile from Hierarchical Clustering. *Astrophys. J.* **1997**, *490*, 493–508.